Review of Designing an Information Processing Ware for a Diabetic Chip "diabetiChip"

Youssef T. AL-sheikh, Ph.D., M.S., C(ASCP),[1,2,3,4] Jared Millington, B.E.,[2] Joseph D. Andrade, Ph.D.,[2] Daniel Bartholomeuz, Ph.D.,[2] Kang Zhang, M.D., Ph.D.[4,5]

Author Affiliations:

[1]Department of Biomedical Informatics, School of Medicine, University of Utah, 26 South 2000 East Suite 5700 HSEB, Salt Lake City, UT 84112, USA

[2]4M Lab, Department of Bioengineering, School of Engineering, University of Utah, 50 S. Central Campus Dr. RM 2480 MEB, Salt Lake City, UT 84112, USA

[3]ManyOne Networks Salt Lake City Office, 28 South 400 East, Salt Lake City, UT 84111, USA

[4]Moran Eye Center, 65 North Medical Drive, Salt Lake City, UT 84132, USA

[5]Department of Ophthalmology and Visual Sciences, School of Medicine, University of Utah, 65 North Medical Drive, Salt Lake City, UT 84132, USA

Abbreviations: (4M Lab) laboratory for monitoring, measurement, and management of the metabolome; (ChemChip) clinical chemistry chip; (diabetiChip) diabetic chip; (ATP) adenosine triphosphate; (NAD) nicotinamide adenine dinucleotide; (NADH) reduced nicotinamide adenine dinucleotide; (NADPH) phosphorylated reduced nicotinamide adenine dinucleotide; (FFL)

firefly luciferase; (ChipWare) chip ware; (SampleWare) sample ware; (ChemWare) chemistry ware; (LightWare) light detection ware; (InfoWare) information processing ware; (MetaWare) metabolic assays ware; (DataWare) data analysis ware; (VisWare) data visualization ware; (PMT) photomultiplier tube; (ChemCD) clinical chemistry CD; (CoA) coenzyme A; (CO_2) carbon dioxide; (FAD) flavin adenine dinucleotide; ($FADH_2$) reduced flavin adenine dinucleotide; (FMN) flavin mononucleotide; ($FMNH_2$) reduced flavin mononucleotide; (RLU) relative light units

Key Words: bioluminescence, light emission, assay calibration, simulation, central nodes of metabolism, visual display, GlucoFaces™, Diabetes Info Portal, Diabetic Chip

Corresponding Author: Youssef T. AL-sheikh, Ph.D., M.S., C(ASCP), Department of Biomedical Informatics, School of Medicine, University of Utah, 26 South 2000 East Suite 5700 HSEB, Salt Lake City, UT 84112, USA, Phone (801) 783-0026, Fax (801) 581-4297, Email YTAL@utah.edu

Acknowledgments: We thank the many individuals who have contributed to the DiabetiChip project. This work was supported by NIH Grant RR17329 (Multi-Analyte Micro-Devices for Biomedical Applications).

Abstract

Miniaturization of clinical chemistry analyzers can empower research conducted to better understand, diagnose, manage, and cure diseases such as diabetes. For the last decade, we have been working on the design and development of miniaturized clinical chemistry devices (ChemChips), including the Diabetic Chip (diabetiChip), which measure a small array of analytes, are small, portable, fast, easy-to-operate, and inexpensive. The chosen analytical method for the diabetiChip uses bioluminescence, which is highly sensitive and specific, and is based on photon counting and specific enzymatic reactions. Bioluminescent reactions were intentionally chosen for analyzing metabolic reactions due to them utilizing some of the central nodes of metabolism, such as adenosine triphosphate (ATP). The analytical processes of the diabetiChip are carried out within a chip ware by four operational wares: sample ware; chemistry ware; light ware; and information processing ware "InfoWare" (further divided into metabolic reactions ware, data analysis ware, and data visualization ware). InfoWare is the focus of this paper; we show the feasibility of using a set of kinase-utilized enzymatic reactions of a firefly bioluminescence-coupled glucose assay in designing a diabetic chip. We also present the concept of GlucoFaces^{TM} in visualizing measurements of the diabetiChip.

Introduction

Miniaturization of clinical chemistry analyzers can empower ongoing research in better understanding, diagnosing, managing, preventing, and curing diseases such as diabetes. For the last decade, we have been working on the design and development of miniaturized multianalytical clinical chemistry devices (ChemChips), including the Diabetic Chip (diabetiChip), that measure a small array of analytes, are small, portable, fast, easy-to-operate, and inexpensive. The analytical principle of the diabetiChip is the measurement of the number of photons emitted from the coupling of an enzymatic reaction specific to the metabolite of concern with a bioluminescent chemical reaction. Bioluminescent reactions were intentionally chosen for analyzing metabolic reactions due to them utilizing some of the central nodes of metabolism, such as adenosine triphosphate (ATP). Also, due to the high sensitivity and specificity of bioluminescent reactions, the diabetiChip can 'cheaply' analyze multiple metabolites from a small sample volume in a relatively short time (few minutes).

Analytical processes of the diabetiChip are carried out within a micro-scale, multi-well chip (ChipWare) by four operational wares (Figure 1): sample processing ware (SampleWare) for processing and transporting the sample; chemistry ware (ChemWare), which constitutes the various chemical assays, deposited in specific analytical wells; light detection ware (LightWare) for detecting and reporting photon counts; and information processing ware

(InfoWare), which correlates the signal to metabolite concentration, performs calibration, estimates analytical error, and displays the relevant information in simple visual patterns.

ChipWare, SampleWare, and LightWare

Chemistry chips can be manufactured in large quantities with relatively low cost. A variety of microfabrication techniques can be used to build arrays of detection wells, where each well contains an independent bioluminescence-based analytical assay.[1,2] Each unique assay is deposited and stabilized in small quantities in individual detection wells. Commercially available silicon photodiodes, avalanche photodiodes, and photomultiplier tube (PMT) arrays designed for low-light detection are ideal for producing small size-detectors to simultaneously measure signals from multiple analytical channels. Our group has focused on PMT-based detectors during chip development processes. We also examined various sample processing methods, such as top-loading, through-flow, hydrogel, plasma separation membrane, and microfluidic channels. However, we developed a total chemistry micro-analytical system (ChemCD), which integrates all wares.[3] The general concept of the ChemCD is to distribute the biological sample from a single sample acquisition chamber to multiple sample-metering chambers via a distribution channel. Each sample-metering chamber would have a passive valve from which the metered sample volume would travel through burst valves and mixing channels, and enter the analytical wells. Since centrifugal pumping can only move the fluid radially outward, the sample chamber has to be facing the

CD's center, and the distribution channel has to spiral outward. Basic design and an advanced design (involving high speed blood separation unit) are illustrated in Figures 2 and 3, respectively. ChemCD can empower the clinical chemistry chip in measuring analyte concentrations in different biological samples and beyond the analytical detectable limit via the automatic filtering and diluting of biological samples.

ChemWare

A reaction that produces photons has many advantages: the problems associated with color perception or wavelength separation are eliminated, as in the case of reflectance colorimetry; no light source is needed, as in the case of fluorescence spectroscopy; no usage of electrodes susceptible to contamination, as in the case of electrochemical analyzers; and less sample volume, a major concern for the patient. Bioluminescence is light produced by compounds undergoing specific oxidation reactions catalyzed by enzymes. Bioluminescence-based measurements are efficient for analyzing metabolites in the micro to sub-microMolar concentration range due to its high sensitivity (generally 100 to 1,000 times more sensitive than common spectroscopic or colorimetric methods). Bioluminescence occurs naturally in some organisms, such as firefly, bacteria, fish, and fungi. Generally, bioluminescent reactions employ an enzyme called "luciferase," which facilitates the oxidation of an energetic substrate, called "luciferin," into an excited state, where it emits a photon. There are many different luciferases and luciferins with at least 30 different known bioluminescent reactions in nature. The

yellow-green (580 nm wavelength) bioluminescence of fireflies (FFL) is based on the enzyme-catalyzed oxidation of firefly luciferin utilizing adenosine triphosphate (ATP) as a highly specific co-reactant (key light inducer). Interactions between the reactants and ATP result in light emission. Moreover, a calibration curve can be obtained for various ATP initial concentrations or any metabolite coupled to ATP via an enzymatic reaction.[4,5]

InfoWare

InfoWare refers to mathematical models and simulation tools for analyzing metabolic networks, including calibration, data analysis, estimation of analytical error, and simple means of presenting multianalytical data in simple visual patterns that are easily interpretable.[6-8] InfoWare is further divided into three complementary units:

1. MetaWare: Analytes appropriate to diagnosing or managing a metabolic disorder (e.g., diabetes), organ dysfunction (e.g., kidney dysfunction), or physiological condition (e.g., lactation, aging, stress, starvation) are selected. Next, biochemical pathways are explored for reaction(s) utilizing each metabolite of interest and can be coupled to one of the bioluminescence analytical platforms. In general, any reaction utilizing a kinase or a dehydrogenase enzyme could be used to couple an analyte to the ATP or NADH/NADPH "NAD(P)H" platform, respectively. If more than one reaction is available, then the most suitable reaction is chosen based on enzyme availability and assay cost.

2. DataWare: First, configured assays are simulated to examine assay feasibility and optimal physical and chemical parameters such as medium acidity and enzyme concentration. Also, mathematical and statistical methods for design of experiments are used to minimize number of required experiments in assay validation. Then, experimental data and calibration curves are analyzed for optimal assay calibration. Finally, a general analytical calibration curve that encompasses the effects of other metabolites is created with the aim of minimizing the number of experiments required to validate and implement assays of related metabolites onboard the chip.
3. VisWare: Metabolic networking features, mentioned above, are further utilized to visually represent data from a collection of analyzed metabolites via simple, but significantly informative, visual patterns. These visual patterns can ease interpretation and provide new insights for understanding disease etiology and pathophysiology.

MetaWare

Metabolism refers to the highly integrated network of chemical reactions that carries out the cellular processes of extracting and controlling energy from the environment and the synthesis of biochemicals and macromolecules. More than a thousand chemical reactions take place in *Escherichia coli* (a single cell-organism).[9-17] Though this array of reactions may seem overwhelming at first glance, its coherent design and its many common motifs show metabolism to be

much simpler. In different words, the number of reactions in metabolism is large but the number of kinds of reactions is relatively small, and the mechanisms of these reactions are usually simple. Furthermore, a group of about a hundred molecules plays a central role in the metabolism of all forms of life; these are often called the central nodes of metabolism.[10] Utilizing the motifs and central nodes to simulate and analyze the metabolic mesh may hold the key to uncover or better understand disease etiology, improve disease treatment or management, or prevent disease.

Most interchanges of activated groups in metabolism are accomplished by a small set of carriers, some water-soluble vitamins, and some key bioenergetic molecules that collectively form the central nodes of metabolism: ATP (phosphoryl carrier); NADH, NADPH, $FADH_2$, and $FMNH_2$ (electron carriers); CoA and lipoamide (acyl carriers); Thiamine pyrophosphate (aldehyde carrier); Biotin (CO_2 carrier); Tetrahydrofolate (1-carbon units-carrier); Adenosylmethionine (methyl carrier); Cytidine diphosphate diacylglycerol (phosphatidate carrier); Nucleoside triphosphates (nucleotides carriers); Ascorbate, the ionized form of vitamin C (a reducing agent); Vitamin B_2 (a precursor of FAD and FMN); Niacin (a precursor of NAD); Pantothenate (a component of CoA); and Glucose (a universal energy currency) along with the carrier uridine diphosphate glucose.

Human disease phenotypes are controlled not only by genes but also by self-organizing networks; including metabolic, regulatory, and signal transduction

networks, which all display system dynamics. These networks can be divided further into sub-networks. For example, the metabolic network can be viewed as two complementary networks; the metabolite network and the enzyme network. When perturbed, these networks alter their output of matter and energy, and can produce either a pathological or a normal phenotype; depending on the environmental context. Study of the dynamics of these networks by approaches such as metabolic control analysis may provide new insights into the pathogenesis and treatment of complex diseases such as diabetes.[18-22]

Most diseases have metabolic origins; which necessitates analyzing certain metabolites to diagnose, manage, or prevent disease.[16,23-65] Moreover, increasing the number of analyzed metabolites is needed to better understand the biochemical basis of disease.[66-81] This necessitates simultaneous analyses of multiple analytes and requires an analytical methodology capable of performing such analyses at relatively low cost.[82-84] Bioluminescence-based analyses can be coupled to a large number of metabolic reactions.[84] The high sensitivity of bioluminescence-based analyses significantly reduces the needed volumes of sample and chemical reagents needed, and thus reduces cost.[84-87]

Since the central metabolite ATP is a key analyte in the FFL bioluminescent platform, a large number of metabolites can be measured by coupling a metabolite-specific reaction that also involves ATP (usually enzymatic reactions utilizing kinase) to the FFL bioluminescence platform. In such coupled reactions,

light emission will also depend on the type of the kinase-utilized enzymatic reaction; whether produces ATP or competes for ATP. In any case (whether ATP is consumed or produced), the amount of emitted light (or photons) can be correlated to the metabolite concentration via generating a calibration curve for the coupled assay.[4,5]

Glucose Assay

Diabetes is a complex metabolic syndrome that is divided further in multiple sub-disease classes. In general, diabetes is characterized by absolute insulin deficiency in the case of type I diabetes, or partial insulin deficiency or insulin resistance in the case of type II diabetes. Insulin can be described as the shuttle that performs and regulates glucose transport into cells. When insulin is deficient, glucose cannot be well utilized. Knowing that glucose is a universal currency for energy exchange within the human body makes diabetes an energy disease affecting functions of the whole body. [88-103] Thus, tight control of blood glucose levels close to normoglycemia is necessary for reducing the frequency of diabetes short-term complications (hypoglycemia and hyperglycemia) and delaying long-term complications. Therefore, developing a glucose assay is the cornerstone for the diabetiChip. Establishing the glucose analytical assay began with searching the metabolic pathways for enzymatic reaction(s) utilizing glucose, which can be coupled to the FFL bioluminescence platform via ATP. Then, preliminary assay protocols were obtained from the literature.[104-116]

DataWare

FFL Bioluminescence-Coupled Glucose Analytical Assay (Dry)

We refer to the simulation of FFL bioluminescent reaction (ATP assay) and FFL bioluminescence-kinase coupled glucose reactions (glucose assay) of the diabetiChip as the dray assay. The main goals of simulation are examining assay feasibility and estimating optimal concentrations for reagents. FFL bioluminescence reaction requires firefly luciferase (FFL), luciferin (LH_2), oxygen (O_2), and ATP in the presence of magnesium ions (Mg^{2+}). ATP utilizes Mg^{2+} and binds rapidly and reversibly on LH_2 to form the complex luciferase-luciferyl-adenylate "FFL-LH_2-AMP" (steps 1-2 in Figure 4). Molecular oxygen oxidizes the complex to produce oxyluciferin (L_{oxy}), AMP, carbon dioxide (CO_2), and light (step 6 in Figure 4). The light emitting reaction is limited by three steps; the first two occur before oxidation:

1. A proton abstraction from luciferin (step 4 in Figure 4).
2. A conformational change of luciferase (step 5 in Figure 4).
3. Dissociation of the luciferase-oxyluciferin complex "FFL-L_{oxy}" (step 7 in Figure 4).[4-5,7]

After a rapid mixing of the reaction's reagents for about 5 milliseconds (ms), a lag phase of 25 ms occurs before light is emitted (Figure 5). The two limiting steps preceding oxidation, mentioned above, are responsible for this delay. Maximum intensity of the emitted light (I_{max}); which is proportional to the ATP

concentration for values lower than 1 micro-Molar, is reached in less than 1 second, but the time necessary to reach half of this value ($I_{max}/2$) is constant (about 100 ms) and independent of the ATP concentration. A steady-state light signal is obtained only for ATP concentrations lower than 10 nanoMolar. As the ATP concentration is increased beyond this value, the peak light intensity increases. Light's decay rate also increases due to the noncompetitive inhibition of luciferase by oxyluciferin; the concentration of which increases when ATP concentration is raised. A nonsteady state kinetics model proposed by Deluca and McElroy, and modified by Gandelman, is used in simulating the ATP assay with *Gepasi Biochemical Simulation* (Figure 6, Table 1).[4-5,7,117] We had prior knowledge of the FFL bioluminescent assay, which is widely used in different analytical fields. Thus, the aim of simulation was verification rather than proving. Based on simulation, optimal concentrations for ATP, luciferin, and firefly luciferase (FFL) were about 650, 1000-3000, and 400-500 µM (Figure 7).

The enzymatic reactions involving glucose utilize the conversion of glucose and ATP to glucose-6-phosphate and ADP via the glucose kinase enzyme (Figure 8). In Figure 9, we present the general kinetic model "YTAL-sheikh's Kinase-Kinetic Model" for the enzymatic reactions that utilize the conversion of an analyte (denoted by i) and ATP to another analyte (denoted by j) and ADP via a kinase enzyme (denoted by ij). These kinase-utilized reactions can be coupled with the FFL bioluminescent reaction's model, discussed above, in simulating the bioluminescence-kinase coupled reactions.

FFL Bioluminescence-Coupled Glucose Analytical Assay (Wet)

ATP and glucose assays were examined experimentally; used assay protocols are listed in Table 2. In each experiment, five assays for each analyte concentration were run for 60 seconds using a TD 20/20 Luminometer. Data points of the ATP and glucose assays were normalized by dividing each data point by the maximal value of the data set. Assays data points at each second were averaged. Each experiment was repeated three times. We present here results of one experiment performed to validate each of the ATP and glucose assays (Figures 10, 11, and 12).

Assay Calibration

A measurement is a set of operations performed to determine the value of a quantity, such as the concentration of blood glucose. Calibration is a comparative measurement aimed toward comparing an analyte concentration from a patient sample with a calibrant that has a known value for the same analyte. Calibrants are either directly prepared from a pure substance via simple procedures or indirectly via a series of comparative procedures when the substance is impure. Thus, the measurement procedure on the patient sample constitutes the last step in a series of comparisons, in which each comparative step adds to the uncertainty of the final result.

Analyte concentration is usually correlated to the level of signal detected by a clinical laboratory analyzer; the signal is scaled by calibration parameters for conversion into concentration units. In the case of POC devices, such as the glucometer, each batch of testing strips has a calibration code that adjusts the scaling parameters to account for variation among batches. However, calibration codes do not account for variation among testing strips within a batch, changes due to storage conditions, or changes in the sensor's accuracy. Measuring the signals from analytical calibrants (or standards) can account for these variations.

Onboard calibration engages treatment of the unknown, unaccounted for random interferences attributable to the patient sample (or biomatrix effects), validation of the chip analytical performance, and estimation of total analytical error (TAE). Onboard calibration incorporates a number of analytical standards to optimize calibration constants. The more calibration constants in the mathematical equation describing the calibration curve(s), the more standards are required. For the purpose of onboard calibration, we make use of one of the advantages of microarrays; availability of a large number of analytical wells. Also, we make use of microfluidics to treat and distribute biological samples to certain wells, and not to distribute them to other wells.

There are various means for assay calibration such as internal standards, standard additions, and spikes. However, via utilizing multianalytical arrays and microfluidic systems (such as the ones discussed above), we are able to employ

the analytical calibration technique "standard additions" for onboard calibration. In addition to the blank, standards with known analyte concentration are mixed with patient sample (Figure 11). By this, most of the interferences and systematic errors, such as biomatrix effects, inter-batch variability, and signal to concentration correlations, are being accounted for.

Different methods can be used for generating calibration curves; integrating total or partial area under the curve, slope determination, and end-point value (Figure 13). An off-board calibration curve for the glucose assay, discussed above, was generated via integrating the area under the curve of normalized relative light units (RLUs) (Figure 14). The calibration curve was fitted using the *Matlab-Curve Fitting Toolbox*[118] (Figures 15, Tables 3).

We have previously studied and tested onboard calibration on the ATP assay. We present here results of this study to show the feasibility of the clinical chemistry chip's onboard calibration methodology: ATP assay was deposited within wells of chips from different batches, light emission was detected using a CCD camera; images were processed using the software program *ImageJ*, and data were analyzed using *Microsoft Excel* and *Matlab*, and calibration curves were generated. Tested detectable ATP assay's linear range was 1-100 μM. Average concentration measurement error was 19%.

No matter what level of success we achieve in accounting for many of the sources of systematic variation, the main challenge we still face is the end-user error. If the end-user has difficulty in following the operational instructions of the device, the user may obtain inaccurate results even if the analytical assays and signal detector were optimal. Likewise, if the end-user has difficulty in interpreting the results, he/she will not be capable of making use of the results in disease diagnosis or management. Therefore, easy operational instructions and simple data visual patterns are necessary for optimal utilization of the clinical chemistry chip. These issues are discussed in the VisWare section of this paper.

VisWare

Multianalytical clinical chemistry data can be displayed via simple patterns, providing ease of interpretation and enabling fast treatment decision-making by the healthcare provider or patient. High-dimensional data visualization presents a large number of dimensions or parameters of the data on a display surface (soft or hardcopy). High dimensional data visualization projects n dimensional data onto a 2D physical medium. Examples of high dimensional data visualization are illustrated in Table 4.[119-125] Consider a 3D scatterplot. Here the data is n-dimensional, 3 axes are selected and laid out on the plane (the physical medium). The n dimensional points are projected on the 2D surface. Hence this is a 3D visualization on the 2D surface. By coloring and shaping the data points, we could argue that a 3D scatterplot is a 5D representation of n-dimensional data on a 2D

surface. Thus, visualizations can be classified based on the intrinsic dimensionality of the logical representation as well as its potential dimensionality by adding in additional data attributes.[125]

Simple visual displays have been the major theme of our philosophy regarding data representation.[126-127] The first author has emphasized the idea of representing diabetes states, symptoms, and measurements via simple facial and iconic data displays in his other publications, such as the paper titled "Public Adventures in Diabetes: Personal Interactivity in a Modern Science Center."[126-128] We have designed a grid or a set of iconic facial displays to represent the diabetiChip's glucose measurements "YTAL-sheikh's GlucoFaces™" along with interactive, educational manual for data visualization and interpretation that will be available soon on the Diabetes Info Portal <http://www.DiabetesInfoPortal.org> (Figure 16).[126-129] The concept of the GlucoFaces™ is simply correlating glucose measurements with facial features. For example, low glucose values can be represented via the degree of tilting the head, high blood glucose values can be represented via the amount of shading pupils of the eyes, normal glucose values by the width of upward lips, which refer to happiness. Also, all glucose measurement are represented on the nose (a longitudinal bar scaled from 0 to 600 mg/dl glucose concentration). Color attributes were also added to the bar to alarm the patient of diabetes state via the conventional alarming colors (green for normal range, yellow for hyperglycemic range, and red for hypoglycemic range). Only the general frame of the GlucoFaces™ and the three fundamental

GlucoFaces™ (normal, hypoglycemic, and hyperglycemic) are shown in Figure 16. All glucose measurements are variations of the three fundamental GlucoFaces™.

In summary, we have demonstrated throughout this paper the processes of developing the diabetic chip, in general, and an information processing ware (InfoWare) for the Diabetic Chip (diabetiChip), in particular. Bioluminescent chemical reactions are highly sensitive and can be coupled with many metabolic reactions via one of the central nodes of metabolism, such as ATP. Assay simulation, experiments, and calibration proved the feasibility of using FFL Bioluminescent-kinase coupled glucose assay in designing a diabetic chip that is highly sensitive, small, portable, disposable, and cheap. Easing data interpretation and glucose monitoring brought about by designing a set of GlucoFaces™.

References

1. Duffy D. Rapid Prototyping of Microfluidic Systems in Poly(dimethylsiloxane). Anal Chem. 1998;70:4974-84.
2. Jo BH, Van Lerberghe LM, Motsegood KM, Beebe DJ. Three dimensional micro-channel fabrication in polydimethylsiloxane (PDMS) elastomer. J Microelectromech Syst. 2000;9:76-81.
3. Daniel A. Bartholomeusz. Development of a Bioluminescence-Based Multianalyte Biosensor: Fabrication and Instrumentation [Dissertation]. SLC (UT): University of Utah; 2005.

4. Brolin S, Wettermark G. Bioluminescence Analysis. Weinheim: VCH; 1992.
5. Campbell AK. Chemiluminescence. Chichester: VCH; 1985.
6. Cerra FB. Role of nutrition in the management of malnutrition and immune dysfunction of trauma. J Amer Coll Nutr. 1992;11:512-8.
7. Eu JY. Bioluminescent assays for galactose and galactose-1-phosphate: Application of immobilized enzymes and kinetic analysis [Dissertation]. SLC (UT): University of Utah; 2000.
8. Vogt W, Nagel D, Sator H. Cluster Analysis in Clinical Chemistry. Chichester: Wiley; 1987.
9. Stryer L. Biochemistry. 4th ed. New York: W. H. Freeman and Company; 1995.
10. Stryer L. Metabolism: Basic Concepts and Design. 4th ed. New York: W. H. Freeman and Company; 1995.
11. Michal G. Biochemical pathways: an atlas of biochemistry and molecular biology. New York: Wiley; 1999.
12. Koolman J, Rohm K. Color Atlas of Biochemistry. New York: Thieme Medical Publishers Inc.; 1996.
13. Mathews CK. Introduction to Metabolism. 3rd ed. Longman; 2000.
14. Jr. DEK. The Seven Pillars of Life. Science. 2002;295:2215-6.
15. Croes D, Couche F, Wodak SJ, van HJ. Metabolic PathFinding: inferring relevant pathways in biochemical networks. Nucleic Acids Res. 2005;33:W326-30.

16. Zimmet PZ, McCarty DJ, de CMP. The global epidemiology of non-insulin-dependent diabetes mellitus and the metabolic syndrome. J Diabetes Complications. 1997;11:60-8.

17. Wolf NI, Smeitink JAM. Mitochondrial disorders: a proposal for consensus diagnostic criteria in infants and children. Neurology. 2002;59:1402-5.

18. Strohman R. Maneuvering in the complex path from genotype to phenotype. Science. 2002;296:701-3.

19. Cohn RM, Roth KS. Biochemistry and Disease: Bridging Basic Science and Clinical Practice. Baltimore: W & W; 1996.

20. Conti DV, Cortessis V, Molitor J, Thomas DC. Bayesian modeling of complex metabolic pathways. Hum Hered. 2003;56:83-93.

21. Davies R, Bartholomeusz DA, Andrade J. Personal Sensors for the Diagnosis and Management of Metabolic Disorders. Engineering in Medicine & Biology Magazine, IEEE. 2003;22:32-42.

22. Nacher JC, Ochiai T, Yamada T, Kanehisa M, Akutsu T. The role of log-normal dynamics in the evolution of biochemical pathways. Biosystems. 2006;83:26-37.

23. Wanner C, Frommherz K, Horl WH. Hyperlipoproteinemia in chronic renal failure: pathophysiological and therapeutic aspects. Cardiology. 1991;78:202-17.

24. Wallace DC. Mitochondrial DNA mutations in diseases of energy metabolism. J Bioenerg Biomembr. 1994;26:241-50.

25. Waddington JL. Neurodynamics of abnormalities in cerebral metabolism and structure in schizophrenia. Schizophr Bull. 1993;19:55-69.

26. Tyfield LA. Galactosaemia and allelic variation at the galactose-1-phosphate uridyltransferase gene: a complex relationship between genotype and phenotype. Eur J Pediatr. 2000;159(Suppl 3):S204-7.

27. Tjoa S, Fennessey P. The identification of trimethylamine excess in man: quantitative analysis and biochemical origins. Anal Biochem. 1991;197:77-82.

28. Schadewaldt P, Killius S, Kamalanathan L, Hammen HW, Strassburger K, Wendel U. Renal excretion of galactose and galactitol in patients with classical galactosaemia, obligate heterozygous parents and healthy subjects. J Inherit Metab Dis. 2003;26:459-79.

29. Ferrannini E. The insulin resistance syndrome. Curr Opin Nephrol Hypertens. 1992;1:291-8.

30. Vanier MT. Lipid changes in Niemann-Pick disease type C brain: personal experience and review of the literature. Neurochem Res. 1999;24:481-9.

31. Kruger G, Haubitz I, Weinhardt F, Hoyer S. Brain oxidative metabolism and blood flow in alcoholic syndromes. Subst Alcohol Actions Misuse. 1980;1:295-307.

32. Jeanrenaud B. Hyperinsulinemia in obesity syndromes: its metabolic consequences and possible etiology. Metabolism. 1978;27:1881-92.

33. Grundy SM. Metabolic syndrome: connecting and reconciling cardiovascular and diabetes worlds. J Am Coll Cardiol. 2006;47:1093-100.

34. Smith JP, Kanekal S, Patawaran MB, Chen JY, Jones RE, Orenberg EK, Yu NY. Drug retention and distribution after intratumoral chemotherapy with fluorouracil/epinephrine injectable gel in human pancreatic cancer xenografts. Cancer Chemother Pharmacol. 1999;44:267-74.

35. Mizoguchi N, Ono H, Eguchi T, Sakura N. Galactose metabolites in blood from neonates with and without hypergalactosaemia detected by mass screening. Eur J Pediatr. 2000;159:851-3.

36. James SJ, Cutler P, Melnyk S, Jernigan S, Janak L, Gaylor DW, Neubrander JA. Metabolic biomarkers of increased oxidative stress and impaired methylation capacity in children with autism. Am J Clin Nutr. 2004;80:1611-7.

37. Dunstan CR, Hills E, Norman AW, Bishop JE, Mayer E, Wong SY, et al. The pathogenesis of renal osteodystrophy: role of vitamin D, aluminium, parathyroid hormone, calcium and phosphorus. Q J Med. 1985;55:127-44.

38. Murphy EJ. Acute pain management pharmacology for the patient with concurrent renal or hepatic disease. Anaesth Intensive Care. 2005;33:311-22.

39. Ma JS, Chen PY, Fu LS, Chi CS, Huang YF, Lin CY, Shieh CC. Chronic granulomatous disease: a case report. J Microbiol Immunol Infect. 2000;33:118-22.

40. Song JC, White CM. Clinical pharmacokinetics and selective pharmacodynamics of new angiotensin converting enzyme inhibitors: an update. Clin Pharmacokinet. 2002;41:207-24.

41. Holme E, Lindstedt S. Diagnosis and management of tyrosinemia type I. Curr Opin Pediatr. 1995;7:726-32.

42. Schaefer F, Straube E, Oh J, Mehls O, Mayatepek E. Dialysis in neonates with inborn errors of metabolism. Nephrol Dial Transplant. 1999;14:910-8.

43. Messiha FS. Extrapyramidal disorders: a possible underlying mechanism. Brain Res Bull. 1983;11:233-41.

44. Perucca E, Grimaldi R, Crema A. Interpretation of drug levels in acute and chronic disease states. Clin Pharmacokinet. 1985;10:498-513.

45. Ziboh VA, Miller CC, Cho Y. Metabolism of polyunsaturated fatty acids by skin epidermal enzymes: generation of antiinflammatory and antiproliferative metabolites. Am J Clin Nutr. 2000;71:361S-6S.

46. Schneider AB, Sherwood LM. Pathogenesis and management of hypoparathyroidism and other hypocalcemic disorders. Metabolism. 1975;24:871-98.

47. Dann HM, Morin DE, Bollero GA, Murphy MR, Drackley JK. Prepartum intake, postpartum induction of ketosis, and periparturient disorders affect the metabolic status of dairy cows. J Dairy Sci. 2005;88:3249-64.

48. Bikle DD. Role of vitamin D, its metabolites, and analogs in the management of osteoporosis. Rheum Dis Clin North Am. 1994;20:759-75.

49. Smith KS, Lee C-L, Ridlington JW, Leonard SW, Devaraj S, Traber MG. Vitamin E supplementation increases circulating vitamin E metabolites tenfold in end-stage renal disease patients. Lipids. 2003;38:813-9.

50. Feksa LR, Cornelio AR, Vargas CR, de SWAT, Dutra-Filho CS, Wajner M, Wannmacher CMD. Alanine prevents the inhibition of pyruvate kinase activity caused by tryptophan in cerebral cortex of rats. Metab Brain Dis. 2003;18:129-37.

51. Diplock AT. Antioxidant nutrients and disease prevention: an overview. Am J Clin Nutr. 1991;53:189S-93S.

52. Widemann BC, Balis FM, Murphy RF, Sorensen JM, Montello MJ, O'Brien M, Adamson PC. Carboxypeptidase-G2, thymidine, and leucovorin rescue in cancer patients with methotrexate-induced renal dysfunction. J Clin Oncol. 1997;15:2125-34.

53. Carlsson A, Fornstedt B. Catechol metabolites in the cerebrospinal fluid as possible markers in the early diagnosis of Parkinson's disease. Neurology. 1991;41:50-1; discussion 2.

54. Tofovic SP, Salah EM, Mady HH, Jackson EK, Melhem MF. Estradiol metabolites attenuate monocrotaline-induced pulmonary hypertension in rats. J Cardiovasc Pharmacol. 2005;46:430-7.

55. Dave-Sharma S, Wilson RC, Harbison MD, Newfield R, Azar MR, Krozowski ZS, et al. Examination of genotype and phenotype relationships in 14 patients with apparent mineralocorticoid excess. J Clin Endocrinol Metab. 1998;83:2244-54.

56. Kelley VE, Ferretti A, Izui S, Strom TB. A fish oil diet rich in eicosapentaenoic acid reduces cyclooxygenase metabolites, and suppresses lupus in MRL-lpr mice. J Immunol. 1985;134:1914-9.

57. Longoni B, Migliori M, Ferretti A, Origlia N, Panichi V, Boggi U, et al. Melatonin prevents cyclosporine-induced nephrotoxicity in isolated and perfused rat kidney. Free Radic Res. 2002;36:357-63.

58. Haussler MR, Cordy PE. Metabolites and analogues of vitamin D. Which for what? JAMA. 1982;247:841-4.

59. Ziolkowska H. Minimizing bone abnormalities in children with renal failure. Paediatr Drugs. 2006;8:205-22.

60. Coen G, Bianchini G, Casciani CU. Physiopathological and therapeutic aspects of vitamin D. Acta Vitaminol Enzymol. 1980;2:103-18.

61. Scharla. Relative value of plain vitamin D and of biologically active vitamin D in the prevention and treatment of osteoporosis. Z Rheumatol. 2006.

62. Cornelio AR, Rodrigues V, de SWAT, Dutra-Filho CS, Wajner M, Wannmacher CMD. Tryptophan reduces creatine kinase activity in the brain cortex of rats. Int J Dev Neurosci. 2004;22:95-101.

63. Lips P. Vitamin D physiology. Prog Biophys Mol Biol. 2006;92:4-8.

64. Scholmerich J, Holstege A. Aetiology and pathophysiology of chronic liver disorders. Drugs. 1990;40(Suppl 3):3-22.

65. Oates, Mylari. Aldose reductase inhibitors: therapeutic implications for diabetic complications. Expert Opin Investig Drugs. 1999;8:2095-119.

66. Lee K, Jin X, Zhang K, Copertino L, Andrews L, Baker-Malcolm J, et al. A biochemical and pharmacological comparison of enzyme replacement

therapies for the glycolipid storage disorder Fabry disease. Glycobiology. 2003;13:305-13.

67. Morganroth J, Levy RI, Fredrickson DS. The biochemical, clinical, and genetic features of type III hyperlipoproteinemia. Ann Intern Med. 1975;82:158-74.

68. Thiele I, Price ND, Vo TD, Palsson BO. Candidate metabolic network states in human mitochondria. Impact of diabetes, ischemia, and diet. J Biol Chem. 2005;280:11683-95.

69. de LP, Cormier-Daire V, Vuillaumier-Barrot S, Cuer M, Durand G, Munnich A, et al. Carbohydrate-deficient blood glycoprotein syndrome. Arch Pediatr. 2000;7:173-84.

70. Koh, Cheung. Cellular mechanism of U18666A-mediated apoptosis in cultured murine cortical neurons: Bridging Niemann-Pick disease type C and Alzheimer's disease. Cell Signal. 2006.

71. Feussner G, Wagner A, Kohl B, Ziegler R. Clinical features of type III hyperlipoproteinemia: analysis of 64 patients. Clin Investig. 1993;71:362-6.

72. Aichberger, Mayerhofer, Vales, Krauth, Gleixner, Bilban, et al. The CML-related oncoprotein BCR/ABL induces expression of histidine decarboxylase (HDC) and the synthesis of histamine in leukemic cells. Blood. 2006.

73. Segal S. Defective galactosylation in galactosemia: is low cell UDPgalactose an explanation? Eur J Pediatr. 1995;154:S65-71.

74. Segal S. Galactosemia unsolved. Eur J Pediatr. 1995;154:S97-102.

75. Sheu KF, Calingasan NY, Lindsay JG, Gibson GE. Immunochemical characterization of the deficiency of the alpha-ketoglutarate dehydrogenase complex in thiamine-deficient rat brain. J Neurochem. 1998;70:1143-50.

76. Klepper J. Impaired glucose transport into the brain: the expanding spectrum of glucose transporter type 1 deficiency syndrome. Curr Opin Neurol. 2004;17:193-6.

77. Coates PM, Tanaka K. Molecular basis of mitochondrial fatty acid oxidation defects. J Lipid Res. 1992;33:1099-110.

78. Huang Z, Hou Q, Cheung NS, Li Q-T. Neuronal cell death caused by inhibition of intracellular cholesterol trafficking is caspase dependent and associated with activation of the mitochondrial apoptosis pathway. J Neurochem. 2006;97:280-91.

79. Seymour CA, Thomason MJ, Chalmers RA, Addison GM, Bain MD, Cockburn F, et al. Newborn screening for inborn errors of metabolism: a systematic review. Health Technol Assess. 1997;1:i-iv, 1-95.

80. Ligler FS, Taitt CR, Shriver-Lake LC, Sapsford KE, Shubin Y, Golden JP. Array biosensor for detection of toxins. Anal Bioanal Chem. 2003;377:469-77.

81. Biagini RE, Smith JP, Sammons DL, MacKenzie BA, Striley CAF, Robertson SK, Snawder JE. Development of a sensitivity enhanced multiplexed fluorescence covalent microbead immunosorbent assay (FCMIA) for the measurement of glyphosate, atrazine and metolachlor mercapturate in water and urine. Anal Bioanal Chem. 2004;379:368-74.

82. Bruenner BA, Jones AD, German JB. Simultaneous determination of multiple aldehydes in biological tissues and fluids using gas chromatography/stable isotope dilution mass spectrometry. Anal Biochem. 1996;241:212-9.

83. Bitton G, Koopman B. Bacterial and enzymatic bioassays for toxicity testing in the environment. Rev Environ Contam Toxicol. 1992;125:1-22.

84. Frantz A, Salla S, Redbrake C. A sensitive assay for the quantification of glucose and lactate in the human cornea using a modified bioluminescence technique. Graefes Arch Clin Exp Ophthalmol. 1998;236:61-4.

85. Salla S, Redbrake C, Frantz A. Employment of bioluminescence for the quantification of adenosine phosphates in the human cornea. Graefes Arch Clin Exp Ophthalmol. 1996;234:521-6.

86. Deo SK, Mirasoli M, Daunert S. Bioluminescence resonance energy transfer from aequorin to a fluorophore: an artificial jellyfish for applications in multianalyte detection. Anal Bioanal Chem. 2005;381:1387-94.

87. Lee J. Bacterial Bioluminescence. Quantum Yields and Stoichiometry of the Reactants Reduced Flavin Mononucleotide, Dodecanal, and Oxygen, and of a Product Hydrogen Peroxide. Biochemistry. 1972;11:3350-9.

88. Doi J, Shiraishi K, Haida M, Matsuzaki S. Abnormality of energy metabolism in the skeletal muscle of patients with liver cirrhosis and changes under administration of glucose and branched-chain amino acids. Tokai J Exp Clin Med. 2004;29:191-8.

89. Hoyer S, Muller D, Plaschke K. Desensitization of brain insulin receptor. Effect on glucose/energy and related metabolism. J Neural Transm Suppl. 1994;44:259-68.

90. Schuster R, Jacobasch G, Holzhutter HG. Mathematical modelling of metabolic pathways affected by an enzyme deficiency. Energy and redox metabolism of glucose-6-phosphate-dehydrogenase-deficient erythrocytes. Eur J Biochem. 1989;182:605-12.

91. Jha B, Pohlit W. Effect of 2-deoxy-D-glucose on DNA double strand break repair, cell survival and energy metabolism in euoxic Ehrlich ascites tumour cells. Int J Radiat Biol. 1992;62:409-15.

92. Levitsky LL, Paton JB, Fisher DE, Delannoy CW. Arterial blood levels of energy substrates and evidence for renal glucose production in the baboon infant. Pediatr Res. 1980;14:926-31.

93. Vlassara H. Advanced glycation in health and disease: role of the modern environment. Ann N Y Acad Sci. 2005;1043:452-60.

94. El-seweidy MM, El-Swefy SE, Ameen RS, Hashem RM. Effect of age receptor blocker and/or anti-inflammatory coadministration in relation to glycation, oxidative stress and cytokine production in stz diabetic rats. Pharmacol Res. 2002;45:391-8.

95. Huang JS, Guh JY, Chen HC, Hung WC, Lai YH, Chuang LY. Role of receptor for advanced glycation end-product (RAGE) and the JAK/STAT-signaling pathway in AGE-induced collagen production in NRK-49F cells. J Cell Biochem. 2001;81:102-13.

96. Hori O, Yan SD, Ogawa S, Kuwabara K, Matsumoto M, Stern D, Schmidt AM. The receptor for advanced glycation end-products has a central role in mediating the effects of advanced glycation end-products on the development of vascular disease in diabetes mellitus. Nephrol Dial Transplant. 1996;11 Suppl 5:13-6.

97. Wang X, Desai K, Clausen JT, Wu L. Increased methylglyoxal and advanced glycation end products in kidney from spontaneously hypertensive rats. Kidney Int. 2004;66:2315-21.

98. Floridi A, Trizza V, Paolotti P, Lucarelli C. Analytical strategy for the assessment of the protein glycation status in uremic patients by high-performance liquid chromatography. J Chromatogr A. 1999;846:65-71.

99. Schleicher E, Wieland OH. Protein glycation: measurement and clinical relevance. J Clin Chem Clin Biochem. 1989;27:577-87.

100. Bruno MR, Sensi M, Cioccia GP, Valente L, Negri M, Ghirlanda G, Pozzilli P. Inhibition of protein non-enzymic glycation induced by Bendazac. Diabetes Res. 1988;9:11-4.

101. Devamanoharan PS, Ali AH, Varma SD. Non-enzymatic glycation of lens proteins and haemoglobin-inhibition by pyruvate: an in-vivo study. Diabetes Obes Metab. 1999;1:159-64.

102. Huby R, Harding JJ. Non-enzymic glycosylation (glycation) of lens proteins by galactose and protection by aspirin and reduced glutathione. Exp Eye Res. 1988;47:53-9.

103. Gao N, Shang J, Lehrman MA. Analysis of glycosylation in CDG-Ia fibroblasts by fluorophore-assisted carbohydrate electrophoresis: implications for extracellular glucose and intracellular mannose 6-phosphate. J Biol Chem. 2005;280:17901-9.

104. Calvert RM, Hopkins HC, Reilly MJ, Forsythe SJ. Caged ATP - an internal calibration method for ATP bioluminescence assays. Lett Appl Microbiol. 2000;30:223-7.

105. Hara KY, Mori H. An efficient method for quantitative determination of cellular ATP synthetic activity. J Biomol Screen. 2006;11:310-7.

106. Liu B-F, Ozaki M, Hisamoto H, Luo Q, Utsumi Y, Hattori T, Terabe S. Microfluidic chip toward cellular ATP and ATP-conjugated metabolic analysis with bioluminescence detection. Anal Chem. 2005;77:573-8.

107. Ishii S, Saito T, Ise K, Sato Y, Tsutiya T, Kenjo A, et al. Evaluation of energy state of islet independent of size using a newly developed ATP bioluminescence assay. Transplant Proc. 2005;37:3499-500.

108. Tani H, Maehana K, Kamidate T. Chip-based bioassay using bacterial sensor strains immobilized in three-dimensional microfluidic network. Anal Chem. 2004;76:6693-7.

109. Young IT, Moreman R, Van Den Doel LR, Iordanov V, Kroon A, Dietrich HRC, et al. Monitoring enzymatic reactions in nanolitre wells. J Microsc. 2003;212:254-63.

110. Chu CP, Lee DJ, Chang BV, and Liao CS. Using ATP Bioluminescence Technique for Monitoring Microbial Activity in Sludge. Biotech Bioeng. 2001;75:469-74.

111. Corbitt AJ, Bennion N, Forsythe SJ. Adenylate kinase amplification of ATP bioluminescence for hygiene monitoring in the food and beverage industry. Lett Appl Microbiol. 2000;30:443-7.

112. Naslund B, Stahle L, Lundin A, Anderstam B, Arner P, Bergstrom J. Luminometric single step urea assay using ATP-hydrolyzing urease. clin chem.. 1998;44:1964-73.

113. Nicolas JC, Terouanne B, Boussioux AM, Crastes DPA. Chemiluminescence and bioluminescence in clinical analysis: Perspectives of development. Ann Biol Clin. 1985;43:201-5.

114. Valat C, Champiat D, Degorce-Dumas JR, Thomas O. Bioluminescence-based assay used for toxicity monitoring. Commun Agric Appl Biol Sci. 2003;68:51-8.

115. Passonneau JV, Lowry OH. Enzymatic Analysis: A Practical Guide. Totowa: The Humana Press Inc.; 1993.

116. Barman TE. Enzyme Handbook. Berlin: Springer-Verlag; 1969.

117. Gepasi.org [homepage on the Internet]. *Gepasi Biochemical Simulation* [updated 2004 Jul 30; cited 2008 Jan 3].

118. The MathWorks [homepage on the Internet]. *Matlab-Curve Fitting Toolbox* [cited 2008 Jan 3]. Available from: http://www.mathworks.com/access/helpdesk/help/toolbox/curvefit/

119. Schreiber F. High quality visualization of biochemical pathways in BioPath. In Silico Biol. 2002;2:59-73.

120. Flury B, Riedwyl H. Multivariate Statistics: A Practical Approach. New York: Chapman and Hall Ltd.; 1988.

121. Green WR. Computer-Aided Data Analysis: A Practical Guide. New York: John Wiley & Sons; 1985.

122. Jacoby WG. Statistical Graphics for Visualizing Multivariate Data. London: Sage Publications Inc.; 1998.

123. Einax JW, Zwanziger HW, Geiss S. Chemometrics in Environmental Analysis. Weinheim: VCH; 1997.

124. Fayyad U, Grinstein GG, Wierse A. Information Visualization in Data Mining and Knowledge Discovery. New York: Morgan Kaufmann Publishers; 2002.

125. Grinstein G, Trutschl M, Cvek U. High-Dimensional Visualizations. KDD. 2001.

126. AL-sheikh YT, Hardman R, Andrade JD. Public Adventures in Diabetes: Personal Interactivity in a Modern Science Center. Diabetes Technology & Therapeutics. 2004;6:61-4.

127. AL-sheikh YT. Multiparameter Data Analysis and Visualization for a Multianalytical Clinical Chemistry – Diabetes Chip [Dissertation]. SLC (UT): University of Utah; 2007.

128. AL-sheikh YT, Andrade JD. Visualizing Multi-Analytical Clinical Diagnostic Data via Simple Patterns [Submitted paper]. AMIA Annual Symposium. November 2008.

129. AL-sheikh YT, Andrade JD, Zhang K. Diabetes Info Portal: A demonstration project for the National Health Information Infrastructure [Accepted Letter to the Editor]. Diabetes Science and Technology. July 2008.

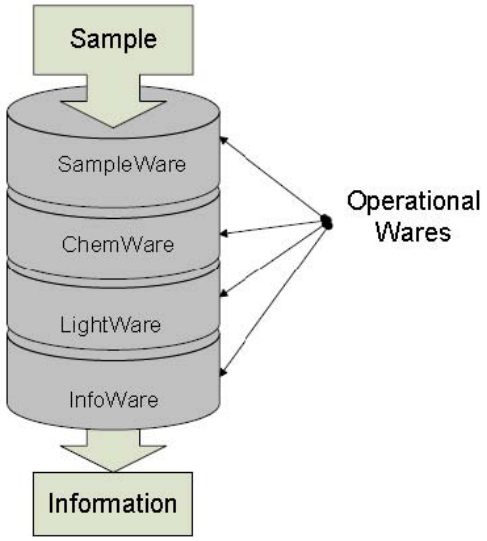

Figure 1: Schematic Representation of the Diabetes Chip's Operational Wares: A biological sample is first processed and distributed to the analytical wells via a SampleWare. Each analytical well contains analyte-specific enzymatic reactions coupled to a bioluminescent reaction. Light signals emitted by reactions from the analytical wells are detected by light-detection elements (LightWare). InfoWare correlates the light signal to analyte concentration and reports results via simple visual patterns.

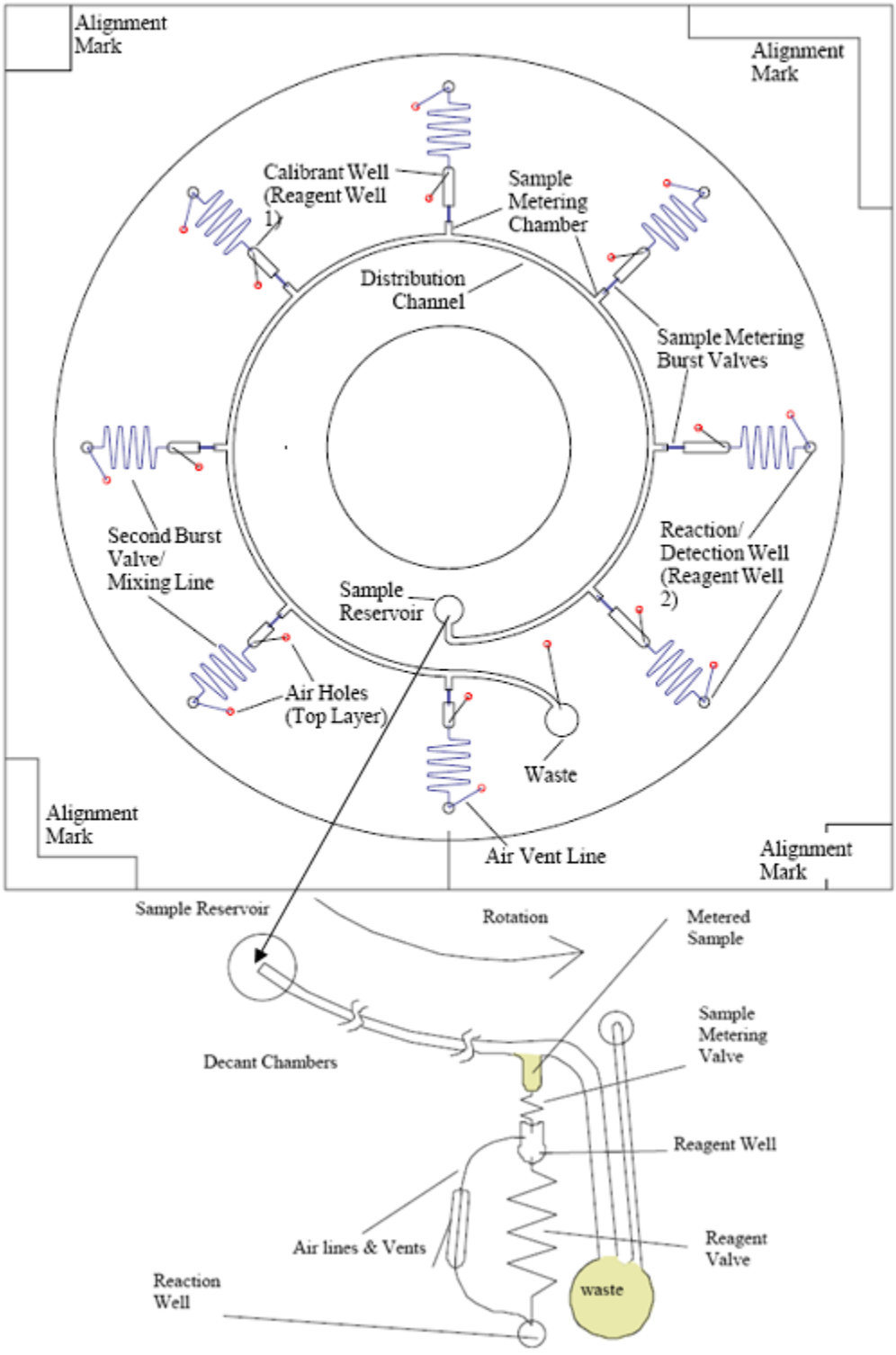

Figure 2: ChemCD Basic Design: Operation of the sample reservoir unit is magnified and detailed.[3]

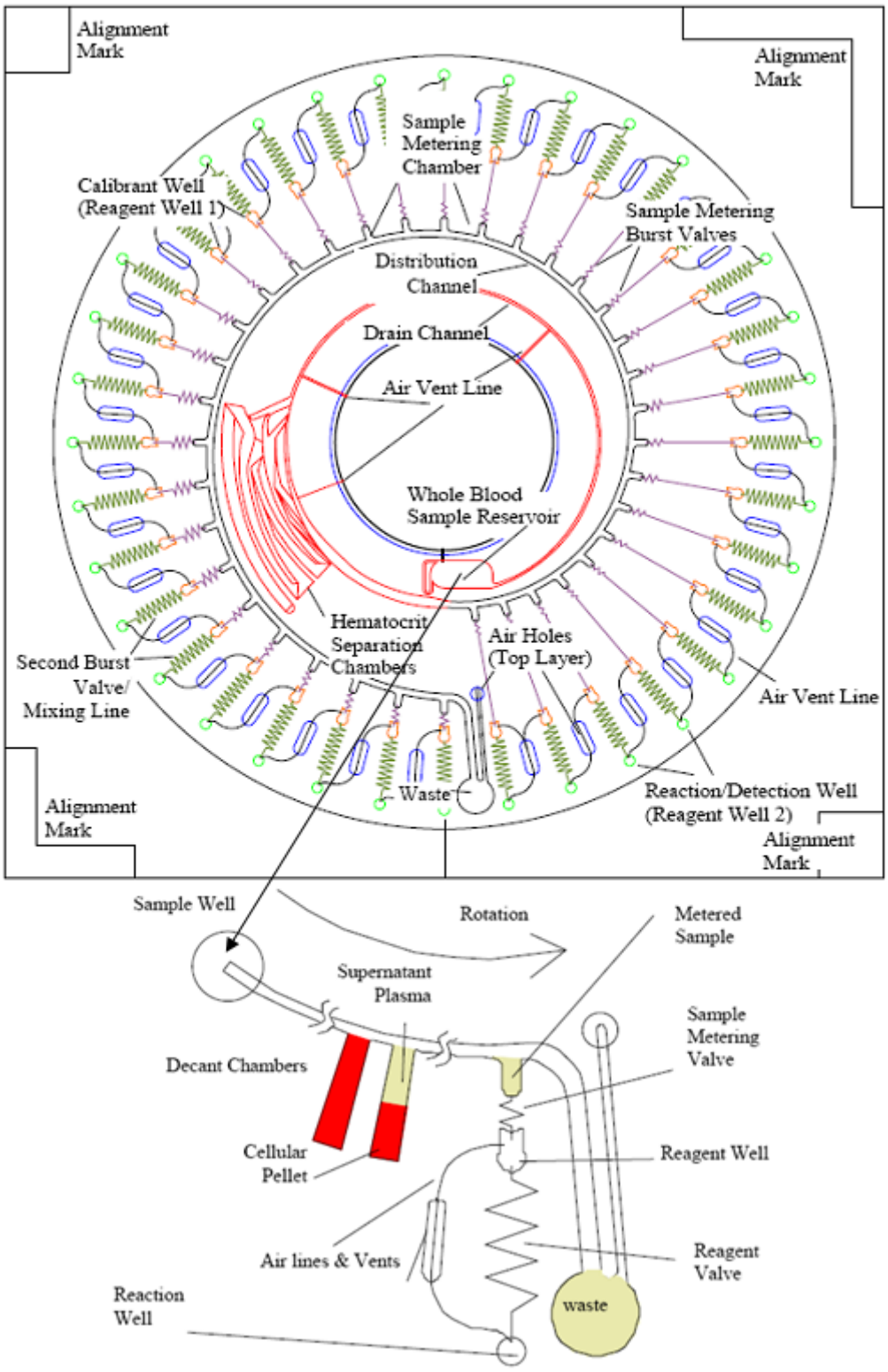

Figure 3: ChemCD Advanced Design: The advanced ChemCD design utilizes a high speed blood separation unit. Operation of the sample reservoir unit is magnified and detailed.[3]

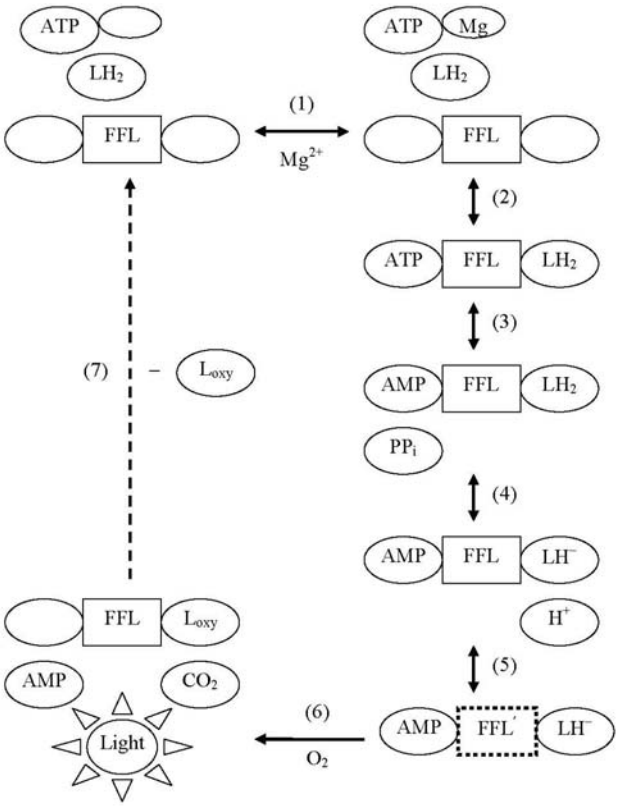

Figure 4: Schematic Representation of the Detailed Steps in a FFL Bioluminescence Reaction.[1-3] ATP firsts bind magnesium ions, which facilitates binding on the enzyme firefly luciferase 'FFL' (Step 1). ATP and luciferin 'LH_2' gets bound to FFL (Step 2). ATP loses orthophosphate and turns into AMP (Step 3). A proton is abstracted from luciferin and conformational change in FFL occurs (Steps 4-5). Steps four and five are responsible for the 25 milliseconds lag phase in light emission. Oxidation of the deprotonized luciferin leads to releasing carbon dioxide (CO_2), AMP, the complex FFL-oxyluciferin, and light (Step 6). Steps six and seven contribute to additional another limitation to light emission; the more oxyluciferin (an inhibitor) is released, the less light is emitted.

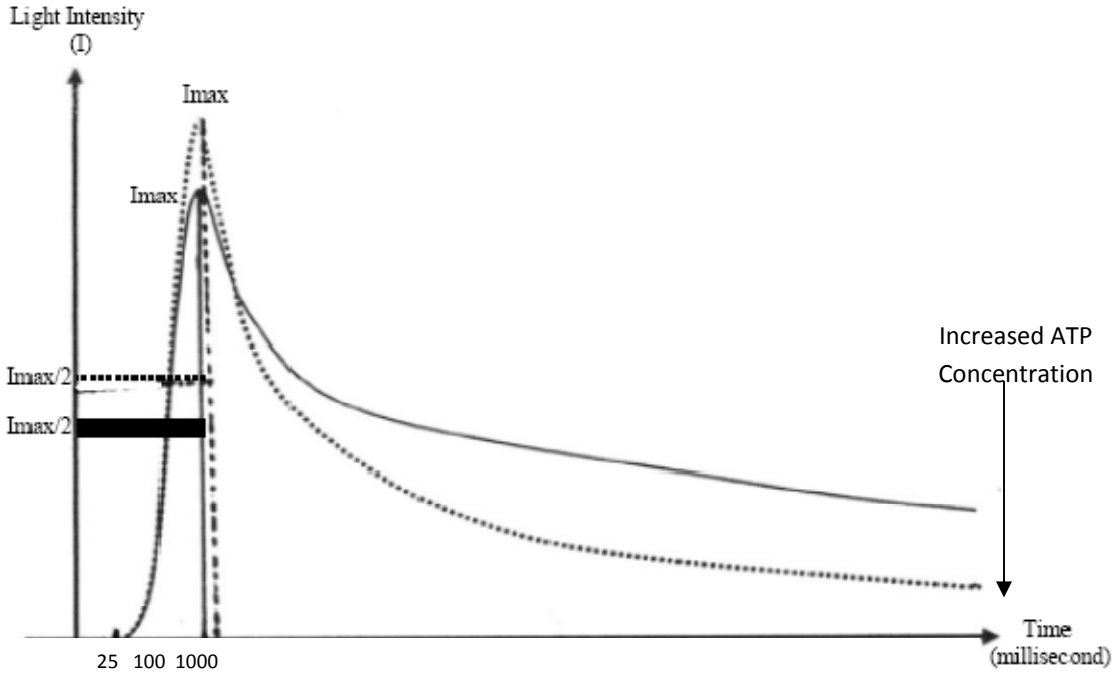

Figure 5: Light Emission Profiles of the FFL Bioluminescent Reaction: The solid curve corresponds to ATP concentrations less than 10 nM. The dotted curve corresponds to ATP concentrations higher than 10 nM. A one half of light intensity is independent of ATP concentration and is always reached after about 100 ms. One the other hand, maximal light intensity depends on ATP concentration. There is a lag phase of about 25 ms in emitting light. The lag phase is mostly due to conformational change in the firefly luciferase enzyme. The light emission decay rate also depends on the concentration of the reaction product oxyluciferin, which is a noncompetitive inhibitor and its concentration is directly correlated with ATP concentration.

$$FFL + ATP \underset{K_{-1}}{\overset{K_1}{\longleftrightarrow}} ATP - FFL \underset{K_{-2}}{\overset{K_2}{\longleftrightarrow}} ATP - FFL - LH_2 \xrightarrow[-AMP,-PP_i]{K_3,O_2}$$

$$FFL - L^*_{oxy} \xrightarrow[-Light]{K_4} FFL - L_{oxy} \underset{K_{-5}}{\overset{K_5}{\longleftrightarrow}} FFL + L_{oxy}$$

Figure 6: The kinetic Model for the FFL Bioluminescence Platform (or ATP assay):[1-3] The first two steps and the last step are reversible and rapid. Rate constants for backward reactions are denoted by minus signs. ATP binds to the enzyme firefly luciferase (FFL) in the first step. FFL binds luciferin (LH_2) in the second step. Luciferin is oxidized and converted to the energetically exited oxyluciferin, and AMP and oxygen are released in the third step. The energetically excited oxyluciferin becomes energetically unexcited and releases the excitation energy in the form of light in the fourth step. Finally, oxyluciferin is dissociated from FFL in the fifth step.

Table 1: Values of the Kinetic Rate Constants Used in Simulating the FFL Bioluminescent Reaction and Bioluminescence-Kinase Coupled Reactions:[1-3] Rows above the double line represent kinetic rate constants of the kinase-specific reaction that is coupled to the FFL bioluminescence reaction, whereas, the rows below the double line corresponds to the kinetic rate constants of the FFL bioluminescent reaction.

Kinetic Rate Constant	Value	Unit
$K_{m(Analyte)i}$ K_{cat}	Specific to the Metabolic Kinase Specific Activity	Molar $\mu mole \cdot mg^{-1} \cdot minute^{-1}$
K_m (ATP)	250×10^{-6}	Molar
K_m (Luciferin)	2×10^{-6}	Molar
K_i (Oxyluciferin)	$\pm 23 \times 10^{-8}$	Molar
K_1	$(10 - 30) \times 10^{3}$	$Molar^{-1} \cdot second^{-1}$
K_{-1}	$(4 - 8) \times 10^{1}$	$Second^{-1}$
K_2	$(5 - 15) \times 10^{5}$	$Molar^{-1} \cdot second^{-1}$
K_{-2}	$(5 - 15) \times 10^{1}$	$Second^{-1}$
K_3	$(20 - 40) \times 10^{1}$	$Second^{-1}$
K_4	$(7 - 13) \times 10^{1}$	$Second^{-1}$
K_5	$(7 - 13) \times 10^{-2}$	$Second^{-1}$
K_{-5}	$(8 - 12) \times 10^{5}$	$Molar^{-1} \cdot second^{-1}$

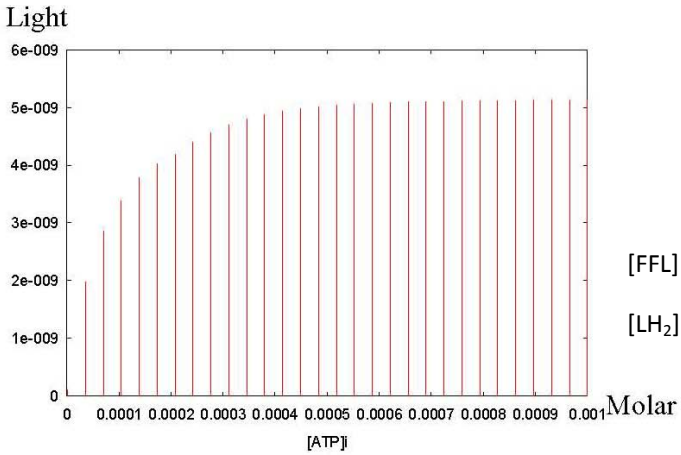

[FFL] = Constant = 0.4 µM

[LH_2] = Constant = 0.1 mM

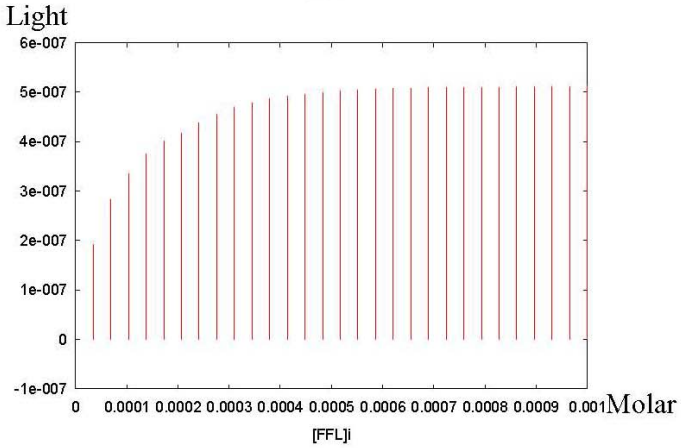

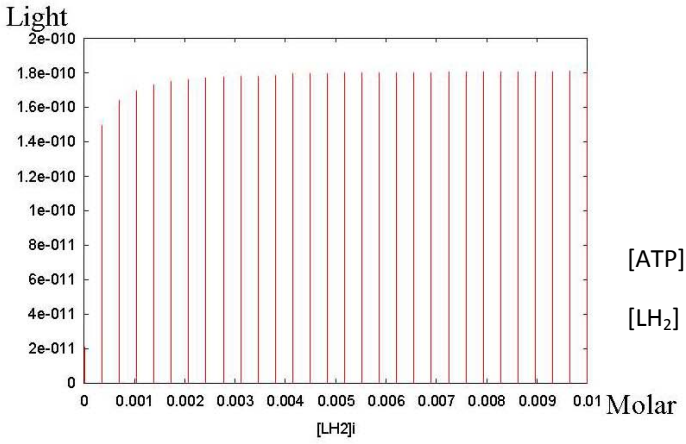

[ATP] = Constant = 0.5 mM

[LH_2] = Constant = 0.1 mM

Figure 7: Optimal Concentrations of ATP, FFL, and Luciferin (LH_2) for the FFL Bioluminescence Platform Found from Reactions Simulation.

$$\mathrm{ATP} + \mathrm{Mg}^{2+} + \mathrm{D\text{-}Luciferin} + \mathrm{O_2} \xrightarrow{\text{Firefly luciferase}} \mathrm{AMP} + \mathrm{Mg}^{2+} + \mathrm{CO_2} + \text{Pyrophosphate} + \text{Oxyluciferin} + \textit{Light}$$

$$\textit{Glucose} + \textit{ATP} \xrightarrow{\textit{Glucose Kinase}} \textit{ADP} + \textit{Glucose} - 6 - \textit{Phosphate}$$

Figure 8: Reactions of the Glucose Assay.

$$(Kinase)_{ij} + (Analyte)_i \xleftrightarrow{k_{-1},k_1} (Kinase)_{ij} - (Analyte)_i$$
$$K_{ij} + x_i \xleftrightarrow{k_{-1},k_1} (K_{ij} - x_i)$$
$$(K_{ij} - x_i) + ATP \xleftrightarrow{k_{-2},k_2} (K_{ij} - x_i) - ATP$$
$$(K_{ij} - Analyte_i) - ATP \xleftrightarrow{k_{-3},k_3} (K_{ij} - Analyte_j) - ADP$$
$$(K_{ij} - x_i) - ATP \xleftrightarrow{k_{-3},k_3} (K_{ij} - x_j) - ADP$$
$$(K_{ij} - x_j) - ADP \xleftrightarrow{k_{-4},k_4} (K_{ij} - x_j) + ADP$$
$$(K_{ij} - x_j) \xleftrightarrow{k_{-5},k_5} K_{ij} + x_j$$
$$-----------------------------$$
$$(K_{ij} - x_i) + ATP \xleftrightarrow{k_{-2},k_2} (K_{ij} - x_i) - ATP \xrightarrow{k_3} (K_{ij} - Analyte_j) - ADP$$
$$I\alpha([ATP]_0 - [ATP])$$
$$d[ATP]/dt = -k_2[(K_{ij} - x_i)].[ATP] + k_{-2}[(K_{ij} - x_i) - ATP]$$
$$d[(K_{ij} - x_i) - ATP]/dt = k_2[(K_{ij} - x_i)].[ATP] - (k_{-2} + k_3).[(K_{ij} - x_i) - ATP]$$
$$[(K_{ij} - x_i) - ATP] = \frac{k_2}{k_{-2} + k_3}[(K_{ij} - x_i)].[ATP]$$
$$d[ATP]/dt = -k_2[(K_{ij} - x_i)].[ATP] + \frac{k_{-2}k_2}{k_{-2} + k_3}[(K_{ij} - x_i)].[ATP]$$
$$d[ATP]/dt = \left\langle \left[-k_2 + \frac{k_{-2}k_2}{k_{-2} + k_3} \right](K_{ij} - x_i) \right\rangle [ATP]$$
$$d[ATP]/dt = \left\langle \left[-\frac{k_2k_3}{k_{-2} + k_3} \right](K_{ij} - x_i) \right\rangle [ATP]$$
$$d[ATP]/[ATP] = \left\langle \left[-\frac{k_2k_3}{k_{-2} + k_3} \right](K_{ij} - x_i) \right\rangle .dt$$
$$[ATP] = [ATP]_0 e^{\left[-\frac{k_2k_3}{k_{-2}+k_3} \right](K_{ij} - x_i).t}$$
$$I\alpha\left([ATP]_0 - [ATP]_0 e^{\left[-\frac{k_2k_3}{k_{-2}+k_3} \right](K_{ij} - x_i).t} \right)$$
$$I\alpha\left(1 - e^{\left[-\frac{k_2k_3}{k_{-2}+k_3} \right](K_{ij} - x_i).t} \right).[ATP]_0$$

Figure 9: YTAL-sheikh's General Kinase-Kinetic Model for Kinase-Utilized Reactions that can be Coupled to the FFL Bioluminescent Reaction.

Table 2: Chemistry Protocols for ATP and Glucose Assays.

Reagent	ATP	Glucose	Glycerol
Glycine-Glycine Buffer	pH = 7.8	pH = 7.8	pH = 7.8
Firefly Luciferase	0.4 µM	0.4 µM	0.4 µM
Magnesium Sulphate	5 µM	5 µM	5 µM
Luciferin	100 µM	100 µM	100 µM
ATP	0, 0.1, 1, 10, 100 µM	500 µM	500 µM
Glucose		0, 25, 100, 200 µM	
Glucose Kinase		2 µM	

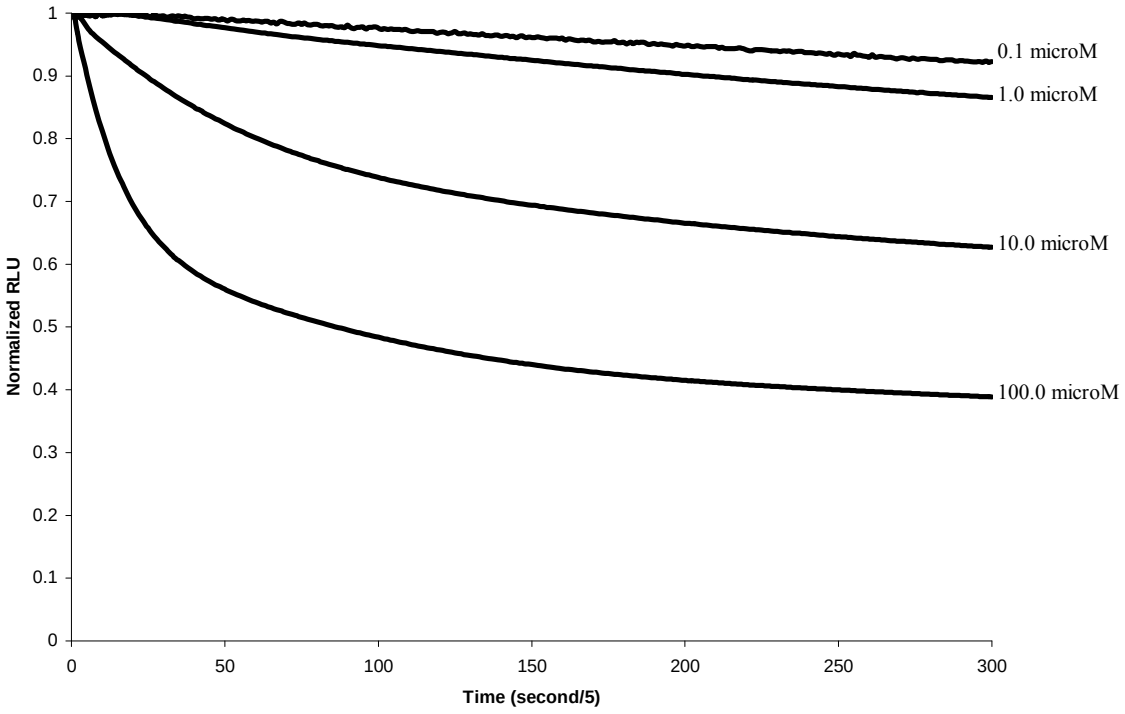

Figure 10: ATP Assay's Light Emission Profiles.

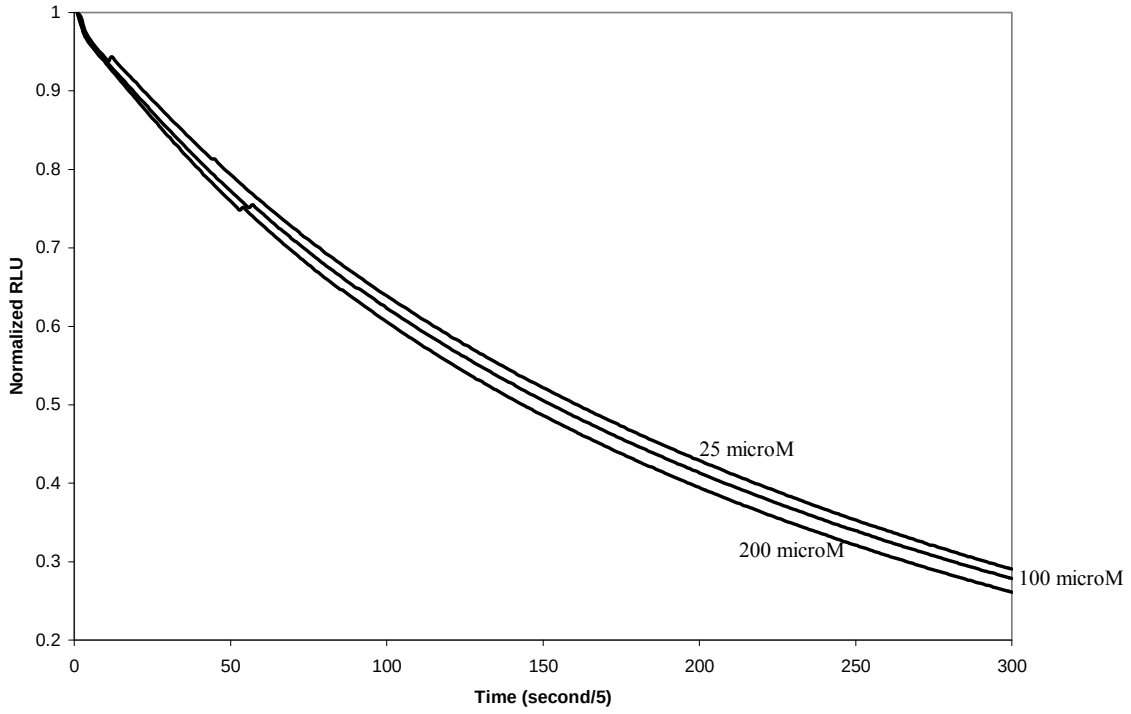

Figure 11: Normalized Light Emission Profiles of the Glucose Assay: Top curve corresponds to 25 micromolar of glucose, middle curve to 100 micromolar glucose, and lowest curve to 200 micromolar glucose.

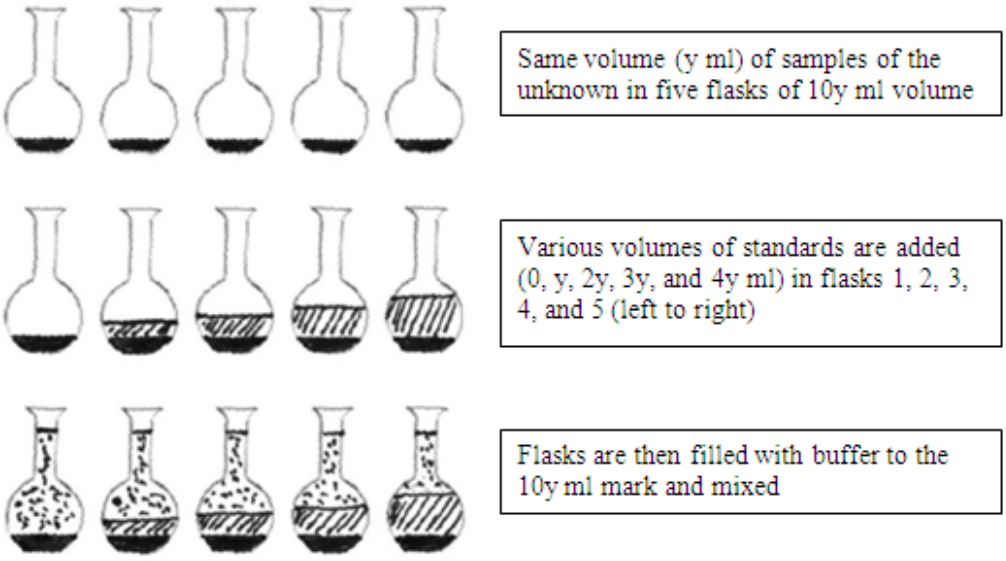

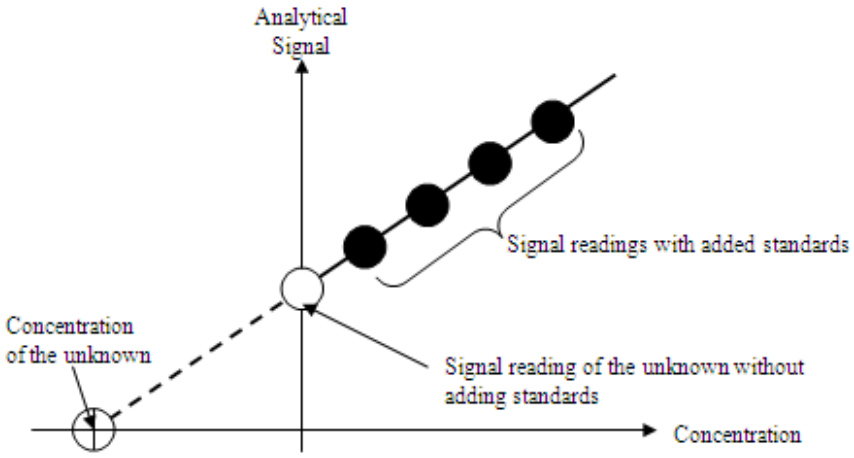

Figure 12: Demonstration of the Standard Additions Assay Calibration Method.

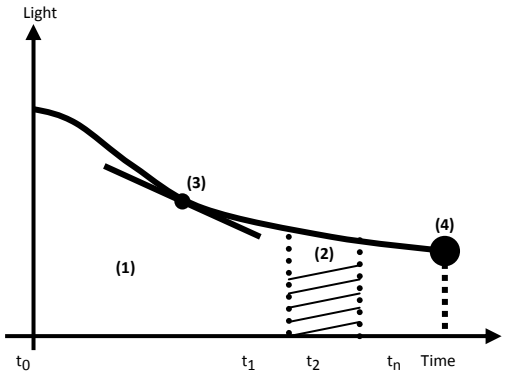

Figure 13: Different Methods for Calibration Curve Analysis and Parameterization: Four methods are shown: Total area under the curve (1), area under the curve between two time points (2), slope value (3), and end point value (4). Method (1) is the easiest as the number of emitted photons, which constitute the area under the curve, can be directly obtained from the light detector. However, if the calibration curve was not graphically examined, potential systematic errors may not be revealed, and thus, total number of emitted photons may not be a valid means for assay calibration. Method (2) can solve ambiguities of method (1); a certain area (between two time points) under the curve is considered instead. Method (3) may be useful if change in analyte concentration can result in noticeable change in the light emission profile. Method (4) resembles method (1) in ease (the last signal reading of the instrument is considered) and also in not recognizing systematic errors. Taking in consideration the pros and cons of these methods, and that experimental light emission profiles agreed with the kinetic model and that no significant systematic errors were noticed, we used the easiest methods (integrating total area under the curve and end point analyses).

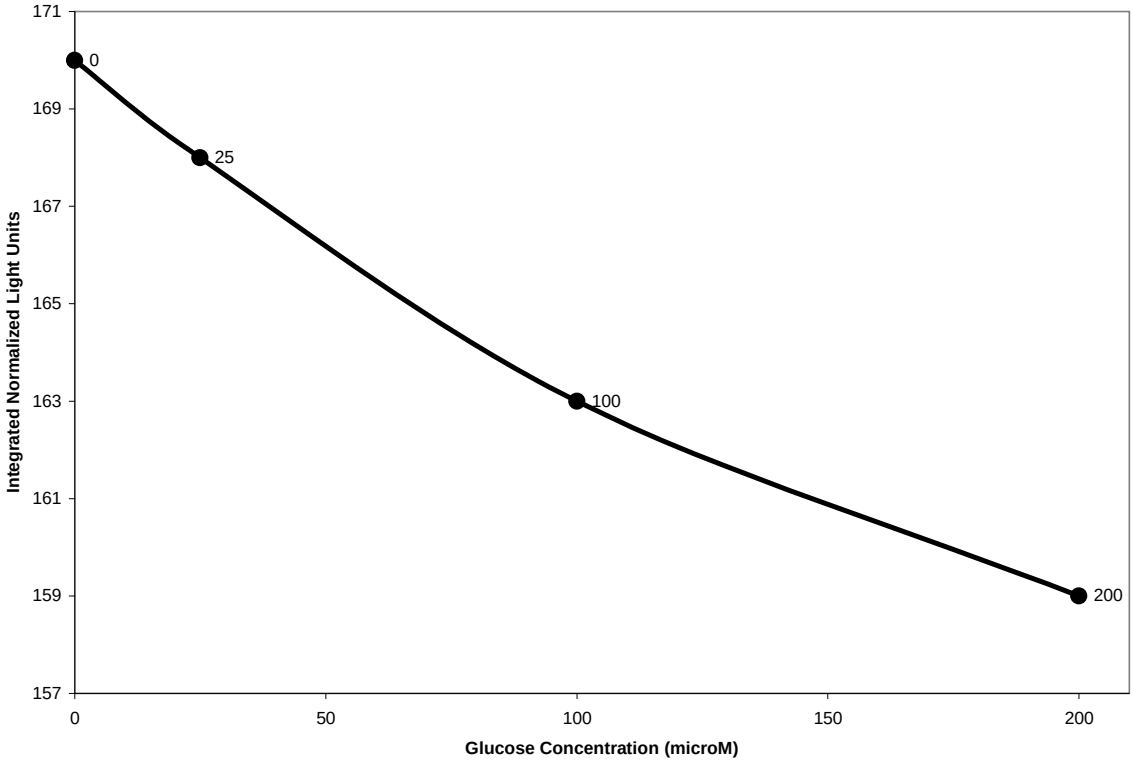

Figure 14: Glucose Assay Calibration Curve.

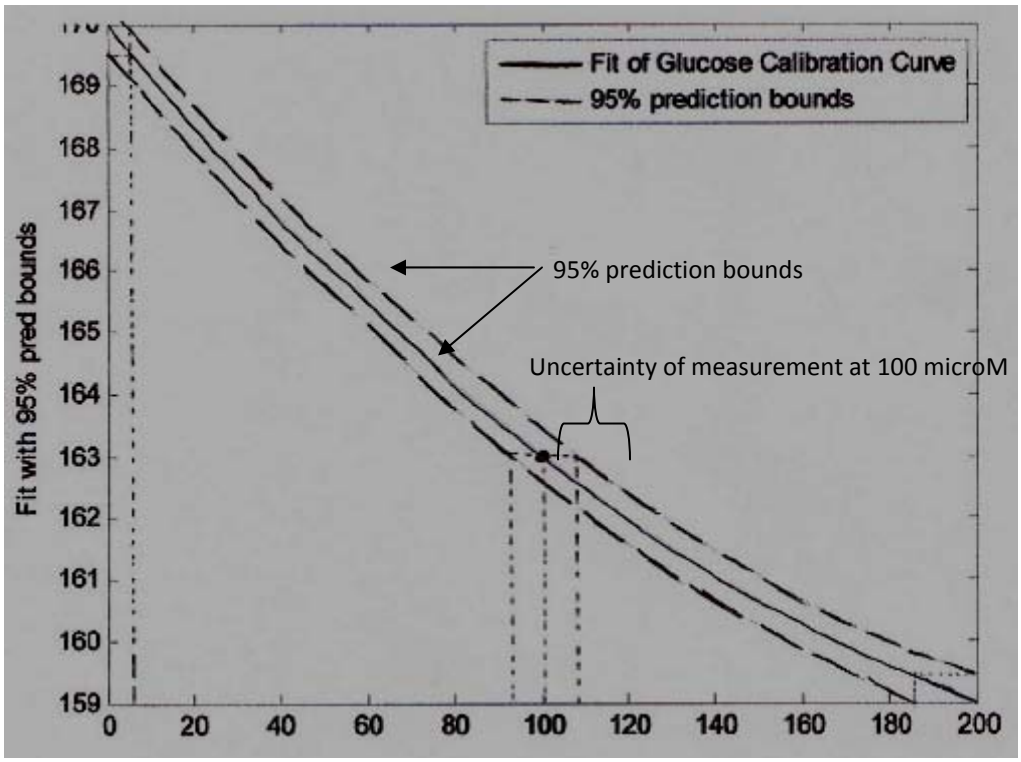

Figure 15: Fitted Glucose Assay Calibration Curve: Assay's analytical detection limits (5–185) micromolar. Uncertainty associated with reporting a 100 micromolar concentration is about ± 5 micromolar.

Table 3: Fitting Model and Parameters, and Goodness of Fit for the Glucose Assay Calibration Curve.

Fitting Model	Quadratic Polynomial $f(x) = p1*x^2 + p2*x + p3$	x is normalized by mean 81.25 and std 89.85
Fitting Parameters	Coefficients (95% confidence) p1 p2 p3	 1.209 (0.9026, 1.514) -5.453 (-5.678, -5.227) 164.1 (163.8, 164.4)
Goodness of Fit	SSE R-square Adjusted R-square RMSE	0.0005988 0.9998 0.9999 0.02447

Table 4: Some Methods of High-Dimensional Data Visualization.[1-7]

Method	Description
2-D or 3-D Scatterplot	A point projection of the data onto a 2D or 3D space. The displayed points can have numerous attributes such as color, size, shape, texture, motion and even sound; when interacted with.
Scatterplot Matrix	An array of scatterplots displaying all possible pairwise combinations of dimensions or coordinates. For n dimensional data this yields n(n −1)2 scatterplots with shared scales.
Heat Map	An array of cells where each cell is colored based on some data value or function on the data.
Height Map	An extension of the heat map with the grid represented as a height field instead of color.
Iconic Display	Each coordinate represents a parameter or attribute of an entity (pixel, icon or glyph) and entities (records) are displayed at once on the screen. There are two types; dimensions of the n-dimensional data set are mapped to certain features of the icon, such as Chernoff faces, where data dimensions are mapped to facial features, or star plots, where the dimensions are represented as equal angular spokes radiating from the center of a circle.
Pixel Technique	An arrangement of the data into an area, starting from some origin, according to the size and number of dimensions, using various techniques including recursive, spiral, and circle segments. The interpretation of the (X, Y) position of the cell depends on the mapping.
Sammon Plot	A non-linear analytic or graphical representation that projects a data set onto a space of lower dimensionality.
Polar Chart	A circular graph for plotting polar coordinates. Polar coordinates map data onto a 2D surface using the angle and radius, creating a wrap-around version of a line graph.
Kohonen Self-Organizing Map (SOM)	A summarization technique that attempts to reduce the complexity of the data set by displaying clusters of the data in a grid. The Kohonen SOM is similar to a k-means clustering algorithm, extending it by providing a topological structure and placing similar objects in neighboring clusters.

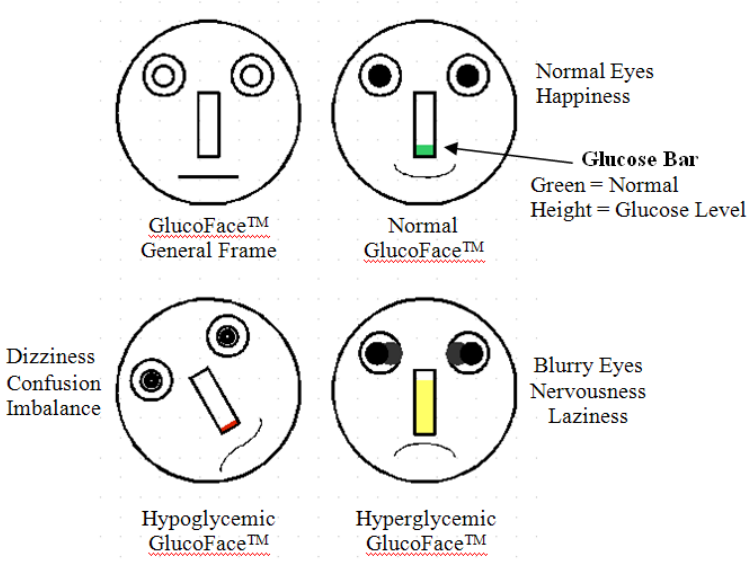

Figure 16: Using Simple Visual Displays (YTAL-sheikh's GlucoFaces™) to Present Results of the diabetiChip.[126-128]